Planetary boundary layer height by means of lidar and numerical simulations~~Boundary Layer variability~~ over New Delhi, India~~, during EUCAARI project~~

Konstantina~~K.~~ Nakoudi[1,~~,~~2], Elina~~E.~~ Giannakaki[1,~~,~~3], Aggeliki~~A.~~ Dandou[1], Maria~~M.~~ Tombrou[1], Mika~~M.~~ Komppula[3]

[1]Department of Environmental Physics and Meteorology, Faculty of Physics, University of Athens, Greece
[2]Alfred Wegener Institute, Helmholtz Centre for Polar and Marine Research, Potsdam, Germany
[3]Finnish~~[3]Fininish~~ Meteorological Institute, Kuopio, Finland

Correspondence to: K. Nakoudi (knakoudi@phys.uoa.gr)

Abstract. In this work, the ~~Ground-based lidar measurements were performed at Gual Pahari measurement station, approximately 20 km South of New Delhi, India, from March 2008 to March 2009. The~~ height of the Planetary Boundary Layer (PBLH) is investigated over Gual Pahari, New Delhi, for almost a year. To this end, ground-based measurements from a multi-wavelength~~PBL) was retrieved with a portable~~ Raman lidar, were used. The ~~system, utilizing the~~ modified Wavelet Covariance Transform (WCT) method was utilized for PBLH retrievals. Results~~. The lidar derived PBL heights~~ were compared to ~~radiosonde~~ data from, Cloud-Aerosol Lidar and Infrared Pathfinder Satellite Observation (CALIPSO) ~~satellite observations~~ and the Weather Research and Forecasting (WRF) model. In order to~~two atmospheric models. The results were also analyzed on a seasonal basis. To~~ examine the difficulties of PBLH~~PBL lidar~~ detection from lidar, we analyzed three cases of PBLH diurnal evolution under different meteorological and aerosol load conditions~~. we focused on three case studies of PBL diurnal evolution.~~ In the presence of ~~a~~ multiple aerosol layers~~layer structure~~, the employed algorithm~~WCT method~~ exhibited high efficiency (r=0.9) in the attribution of PBLH, whereas weak aerosol gradients induced high variability in PBLH. A sensitivity analysis corroborated the stability of the utilized methodology. The ~~PBL height determination. Good agreement with the European Center for Medium-range Weather Forecasts (ECMWF) and the Weather Research and Forecasting (WRF) estimations was found (r=0.69 and r=0.74, respectively) for a cumulus convection case. In the aforementioned cases, temperature, relative humidity and potential temperature radiosonde profiles were well compared to the respective WRF profiles. The Bulk Richardson Number scheme, which was applied to radiosonde profile data, was in good agreement with lidar data, especially during daytime (r=0.68). The overall~~ comparison with CALIPSO ~~satellite~~ observations yielded~~; namely, CALIOP Level 2 Aerosol Layer Product, was very~~ satisfying results (r=0.8~~8~~4), with CALIPSO ~~Feature Detection Algorithms~~ slightly overestimating PBLH. Due to the relatively warmer and drier winter and, correspondingly, colder and rainier pre-monsoon season,~~PBL height. Lidar measurements revealed that the maximum PBL height was reached approximately three hours after~~ the seasonal PBLH~~solar noon, whilst the daily evolution of the PBL was completed, on average, one hour earlier. The PBL diurnal~~ cycle during the measurement ~~was also analyzed using ECMWF estimations, which produced a stronger cycle during the winter and pre-monsoon~~ period was slightly weaker~~. The seasonal analysis of~~

Formatted

Formatted: English (United States)

Formatted: English (United States)

~~lidar PBL heights yielded a less pronounced PBL cycle~~ than the cycle~~one~~ expected from long~~-~~term climate records. ~~The lowest mean daytime PBL height (695 m) appeared in winter, while the highest mean daytime PBL height (1326 m) was found in the monsoon season as expected. PBL daily growth rates exhibited also a weak seasonal variability.~~

1 Introduction

The Planetary Boundary Layer (PBL) is the lowermost portion of the troposphere, which experiences a diurnal cycle of temperature, humidity, wind and pollution variations. ~~The~~ PBL ~~height~~ is a key component of the atmosphere and of the climate system, as it fundamentally affects cloud processes, as well as land and ocean surface fluxes. The PBL height (PBLH) is the most adequate parameter to represent the PBL.~~-~~ Therefore, it is usually required in numerous applications. For~~;~~ ~~for~~ instance, in pollution-dispersion modelling~~modeling~~, where the upper boundary of the turbulent layer acts~~plays a role~~ as an impenetrable lid for the pollutants emitted~~released~~ at the surface. The PBLH~~PBL height~~ also appears as a mixing scale height in turbulence closure schemes within climate and weather prediction models (Zilitinkevich and Baklanov, 2001). As air pollution becomes more severe due to economic development, particularly in developing countries (Wang et al., 2009),~~observations of the PBL height with~~ high temporal and vertical resolution observations of the PBLH are essential for weather and air-quality prediction and research. Moreover, the PBLH~~PBL height~~ is related to the warming rate caused by enhanced greenhouse gases emissions (Pielke et al., 2007).

Several methods have been proposed to estimate the PBLH~~PBL height~~, utilizing vertically resolved thermodynamic variables, turbulence-related parameters and concentrations of tracers (Seibert et al., 2000; Emeis et al., 2004). Different methods for the determination of the PBLH from radiosondes have been compared and the associated uncertainties have been estimated (Seidel et al., 2010; Wang and Wang, 2014). ~~Lidar (Light Detection And Ranging)~~Restrictions of radiosondes refer to the coarse vertical resolution of standard meteorological data with respect to boundary layer studies as well as the smoothing due to the sensor lag constant bounded by the high ascent rate of the radiosonde (Seibert et al., 2000). Remote sensing systems such as aerosol lidar, microwave radiometer (Cimini et al., 2013), wind-profiling radar (Cohn and Angevine, 2000) and Doppler wind lidar (de Arruda Moreira et al., 2018) are suitable for long-term~~can provide continuous~~ measurements of various atmospheric quantities with high temporal resolution and can be used either independently or synergistically to retrieve the PBLH. Space-borne lidar systems provide the advantage of spatial coverage, although for studies focusing on a particular area of interest, measurements are constrained by the overpass frequency. Ceilometers are simple backscatter lidars, which entail less operational cost. However, exploitation of their full potential is on an early stage with limited ceilometer-related studies (Münkel et al., 2007, Binietoglou et al., 2011, Wiegner~~, including the vertical distribution of~~ et al., 2014). Ceilometers have high potential of contributing to PBLH climatology, within certain limits, but detailed investigation of open issues is still needed, as for example, the treatment of incomplete overlap. Additionally, no adjustments can be typically made by the user, contrary to the modified Wavelet Covariance Transform (WCT) algorithm. Hence, improvements on layer detection algorithms are urgently needed to fully exploit the potential of ceilometers. In elastic and Raman lidar systems,

Formatted: Font: 10 pt

the atmospheric aerosols are used as tracers and the PBLH is indicated by a gradient in the range-corrected lidar signal~~from which the PBL height can also be retrieved~~ (Menut et al., 1999; ~~Cohn and Angevine, 2000;~~ Brooks 2003; Amiridis et al., 2007; Morille et al., 2007; Baars et al., 2008; Engelmann et al., 2008; Groß et al., 2011; Tsaknakis et al., 2011; Haeffelin et al., 2012; ~~Cimini et al., 2013;~~ Scarino et al., 2013; Summa et al., 2013; Korhonen et al., 2014; Lange et al., 2014; Bravo-Aranda et al., 2016). Weather and climate prediction models could alternatively be used to determine the PBLH, especially for strong horizontal inhomogeneity. However, inconsistencies in the definition of PBLH among the existing meteorological models also result in significant differences in its calculation (Tombrou et al., 2007).~~; de Arruda Moreira et al., 2018). Atmospheric aerosols are used as tracers and the PBL top is indicated by a gradient in the range-corrected lidar signal.~~

New Delhi is one of the most densely populated cities~~, with 29259 inhabitants per square mile,~~ and the fifth most populous city in the world according to United Nations population estimates and projections of major Urban Agglomerations (https://esa.un.org/unpd/wup/).~~), with an estimated 2016 population of 18.6 million.~~ It is surrounded by the Thar Desert to the west and the western Indo-Gangetic Plain to the north. Particulate air pollution in this area is assumed to originate from fossil fuel and biomass burning besides natural sources such as desert dust (Hedge et al., 2007; Ramanathan et al., 2007a). The identification of the layer height within which pollutants are trapped is particularly important in this polluted area, since the largest and most persistent pollution haze covers an area of about 10 million km^2 over Southern Asia (Nakajima et al., 2007; Ramanathan et al., 2007a). Thus, vertically resolved observations are indispensable to reveal information regarding local air quality, climate change and human health related issues.

Despite the importance of the area under investigation, only few ground-based measurements of aerosol vertical profiles have been carried out, with most of the available data accessed during short field campaigns (Lelieveld et al., 2001; Nakajima et al., 2007; Ramanathan et al., 2007a). In this study, we investigate PBLH~~PBL~~ characteristics over New Delhi, India, based on one~~-~~year long ground-based lidar measurements. The measurements were carried out from March 2008 to March 2009 in the framework of EUCAARI (European Integrated project on Aerosol Cloud Climate and Air Quality Interactions) project (Kulmala et al., 2011).

2 Measurement site

The lidar measurement site was located at Gual Pahari (28.43ºN, 77.15ºE, 243 m a.s.l~~A.S.L.~~), which is situated in the Gurgaon district of Haryana state, about 20 km south of New Delhi, India (Hyvärinen et al., 2010; Komppula et al., 2012). The surroundings of the station represent a semi-urban environment with agricultural test fields and light vegetation. There were no major pollution sources, except for the road between Gurgaon and Faridabad about 0.5 km to the south-west of the station, while only electric-powered vehicles were allowed at the station area. Anthropogenic sources in the greater region comprised traffic, city emissions and power production (Reddy and Venkataraman, 2002a, b).

During the measurement period, sunrise time varied between 5:45 and 7:15 LST, whilst sunset appeared between 18:15 and 19:15 LST. Solar noon appeared between 12:00 and 12:30 LST. Local time at New Delhi corresponds to UTC+5.5 h. From now on in this paper, UTC will be adopted, to

Formatted: Font color: Custom Color(RGB(20,19,20))

facilitate~~since~~ the comparison between the ~~synchronization of results from~~ lidar measurements and Temperature and precipitation patterns can potentially reflect the state of sensible and latent heat fluxes within the PBL as well as the exchange of moisture and momentum with the Earth's surface. Thus, climatologies of meteorological parameters can be considered a valuable tool for assessing the representativeness of PBLH seasonal cycle with respect to long-term measurements. Such a comparison is performed in Section 4.4 based on the 30-year anomalies of maximum temperature and accumulated precipitation (Figure 1).~~In 2008, the highest temperature was recorded in May, with a monthly maximum temperature of 36.9 °C. The annual mean temperature was 24.6 °C in 2008 and 25.4 °C in 2009. Monthly maximum temperatures during May and June were 3 to 4 °C lower than the climatological values (World Meteorological Organization, http://worldweather.wmo.int/en/city.html?cityId=224), while February and March (temperature average of March 2008 and March 2009) were characterized by almost 3 °C higher maximum temperatures, as shown in Figure 1(a). The year 2008 exhibited the most rainfall, between June and September, compared to the four year period 2006-2009, with a total of 570 mm in Gual Pahari (Hyvärinen et al., 2010). However, rainfall (June-September) was lower than the climatological value of 602 mm in New Delhi. In the monthly periods from April to June and August to September 2008, the total precipitation was higher than the one expected from climatology, with a maximum anomaly appearing in May, whereas in July 2008 cumulative precipitation was lower (Figure 1(b)). This year also exhibited an early monsoon onset date on 16 June, which was one of the earliest onset dates recorded in the area with rainfall data available since 1901 (Tyagi et al., 2009). The Indian summer monsoon in 2008 was somewhat weaker than normal, following the La Niña condition in the tropical Pacific (Lau et al., 2009).~~

3 Methodology and Instrumentation~~3 Methods~~

3.1 Ground-based lidar measurements

3.1.1 FMI-Polly^{XT} lidar system

The measurements were conducted with a six-~~-~~channel Raman lidar called FMI-Polly^{XT} (Finnish Meteorological Institute - Portable Lidar sYstem eXTedend). The lidar system was entirely remotely controlled via an internet connection, with all the measurements, data transfer and built-in device regulation being performed automatically. The instrument was equipped with an uninterruptible power supply (UPS) and an air conditioning system (A/C) to allow for safe and smooth continuous measurements. A rain sensor was also connected to the roof cover in order to assure a proper shutdown of the instrument during rain.

FMI-Polly^{XT} ~~lidar~~ used a Continuum Inline III type laser. The pulse rate of the laser was 20 Hz and it delivered energies of 180, 110 and 60 mJ simultaneously (with external second and third harmonic generators) at three different wavelengths, i.e. 1064, 532, 355 nm, respectively. A beam expander was used so as to enlarge the beam from approximately 6 mm to 45 mm. The remaining beam divergence after expansion was less than 0.2 mrad. The backscattered light was collected by a Newtonian telescope, which had a main mirror with a diameter of 30 cm and a field of view of 1 mrad. ~~The vertical resolution of the system was 30 m and the vertical range covered the whole troposphere under~~

~~cloudless conditions.~~ The output of the instrument included vertical profiles of the particle backscatter wavelengths, i.e. 355, 532 and 1064 nm (retrieved with the Klett method; Klett (1981) and Klett (1985)),~~,~~ extinction coefficient at 355 and 532 nm (retrieved with the Raman method (Ansmann et al., 1990; Ansmann et al., 1992) by using the Raman shifted lines of N_2 at 387 and 607 nm) and linear particle depolarization ratio at 355 nm. The system vertical resolution was 30 m and the vertical range covered the whole troposphere under cloudless conditions. This is sufficient for PBL studies considering the heights needed in this work. Engelmann et al. (2016) reports a maximum vertical range of 40 km, which depends on the capabilities (height bins) of the data acquisition. The FMI-Polly^{XT} lidar system is described in more detail in Althausen et al. (2009) and Engelmann et al. (2016).

The incomplete overlap between the laser beam and the receiver field of view L-R (Laser-Receiver), restricted the observational detection range to heights above 200-300 m. This was partly counterbalanced by the overlap correction function. In this study, overlap corrections were performed at 532 nm following the methodology proposed by Wandinger and Ansmann (2002). During the measurement campaign, the L-R overlap was completed at 550-850 m, with the estimation of the full overlap height performed five times, since changes in the system could have affected the alignment between the laser beam and the receiving telescope optical axes.

During night-time, the configuration ~~Table 1 presents the relevant properties~~ of FMI-Polly^{XT} allowed the determination of the Residual Layer height (RLH). The study of Wang et al. (2016) which was performed at a station of similar latitude, Wuhan, China, revealed that the RLH lies mostly in the range 0.5–1.3 km, following a seasonal variation. Hence, for most of our night-time cases we considered that the lidar system detected the top of the residual layer, which contained the aerosol of the previously mixed layer. In particular, if a layer top more than 500m was detected between sunset and sunrise, it was associated with the RLH. ~~, together with the properties of the other techniques utilized. The other techniques will be discussed in the following Sections.~~

Formatted: English (United Kingdom)
Formatted: Font: Bold, English (United Kingdom)
Formatted: Adjust space between Latin and Asian text, Adjust space between Asian text and numbers
Formatted: English (United Kingdom)

3.1.2 PBLH~~PBL top~~ detection technique

The PBLH~~PBL height~~ was derived from the 15~~-~~min averaged lidar backscatter signals at 1064 nm using the ~~wavelet covariance transform (~~WCT~~)~~ method (Brooks, 2003) with modifications introduced by Baars et al. (2008). The algorithm of the WCT method was applied to 6-hour datasets. An overview of the lidar range-corrected signal was made available by TROPOS (Leibniz Institute for Tropospheric Tropospheric Research) and can be accessed at http://polly.rsd.tropos.de/?p=lidarzeit&Ort=21.~~(2008).~~ http://polly.rsd.tropos.de/?p=lidarzeit&Ort=21.~~(2008).~~ The WCT method makes use of the assumption assumption that the PBL contains much more aerosol load compared ~~to~~ the free troposphere and, thus, troposphere and, thus, a strong backscatter signal decrease can be considered as~~observed at~~ the The covariance transform $W_f(a,b)$ is based on~~a measure of~~ the convolution of~~similarity between~~ the signal and the related Haar function (Baars et al., 2008). This method was chosen because it allows allows larger adjustability than other techniques, as shown from previous studies (Baars et al., 2008; al., 2008; Korhnonen et al., 2013~~2014~~). For instance, the gradient technique involves an ambiguity in

Formatted: English (United States)
Formatted: English (United States)
Formatted: English (United States)
Formatted: English (United States)
Formatted: English (United States)
Formatted: English (United States)

ambiguity in the choice of the ~~"~~relevant~~"~~ minimum in the gradient that corresponds to the PBLH PBLH ~~boundary layer height~~ (Lammert and Bösenberg, 2005).

the WCT threshold, ~~threshold value of the WCT~~ which allowed~~permits~~ the identification of ~~a~~ corresponding omission of weak gradients. ~~was introduced as a first modification.~~ The first height maximum of $W_f(a,b)$ occurred, exceeding the selected~~a~~ signal decrease threshold, was defined as the defined as the PBLH. A second modification introduced by Baars et al. (2008) was related to strong gradients ~~PBL height. This threshold was modified~~ in ~~cases of multiple aerosol layers structures, where strong gradients inside the PBL complicated the d~~detection of the PBL height. ~~Furthermore, the option to cut~~ the lower parts of the PBL (30-870 m) and the ability to exclude these parts from the lidar data evaluation. In this work, the ~~signal (from 30 to 870 m) was utilized so as to avoid strong gradients related to the incomplete overlap in the lower heights. The importance of a proper threshold adjustment is discussed in Section 4.1, where three case studies are analyzed and the~~ applicability of the WCT technique~~method,~~ under different meteorological and aerosol load conditions is discussed (Section 4.1) in the context ~~o~~f three case studies and the stability of the WCT algorithm~~,~~ is assessed as well (Section 4.2). Additional cases, where the importance of a proper threshold and cutting-off zone are discussed, can be found in Nakoudi et al. (2018). ~~examined.~~

Daily mean and maximum PBLH corresponds~~PBL heights correspond~~ to convective hours (3:00-12:00 UTC). The hourly PBLH was~~PBL height values were~~ calculated from the 15- min lidar observations~~data~~ by averaging of the three closest data points of the time considered (e.g. 12:00 hourly height would be the average of the three data points between 11:45 and 12:15). The seasonal cycle study was based on the classification proposed by the Indian Meteorological Department, i.e. winter (December-March), pre-monsoon or summer (April-June), monsoon (July-September) and post-monsoon (October-November) (Perrino et al., 2011). However, the PBLH~~PBL~~ seasonal cycle was examined during the winter, pre-monsoon and monsoon periods, as no sufficient data coverage was found during the post-monsoon period (Section ~~. The diurnal PBL cycle is provided by lidar measurements and ECMWF estimations for the whole measurement period as well as on a seasonal basis (Section 4.~~3.1.3). ~~).~~

3.1.3 Data coverage

During the one- ~~-~~year long measurement campaign, ~~from 12 March 2008 to 31 March 2009,~~ FMI-Polly^{XT} was measuring on 139 days. Due to technical problems with the laser, ~~(27%),~~ the data coverage from September to January was sparse. Furthermore, precipitation prohibited lidar measurements, since the lidar system had to shut down. Hence, sufficient ~~(12%). Thus, lidar measurements were possible in 61% of the total time (139 days).~~

~~Sufficient~~ data availability ~~(more than 25%, from 4 h after sunrise to 1 h before sunset)~~ was achieved during 72 days. Multiple~~During these days, multiple~~ aerosol layers appeared mainly between March ~~layer structures (20%)~~ and May, whereas low clouds were present mostly in the monsoon period and both~~(15%)~~ complicated PBLH~~PBL height~~ detection. Additionally, some technical issues arose due to photomultiplier supersaturation and signal problems. ~~(9%).~~ A lack of a significant decrease in the backscatter profile was observed in only a few cases. ~~(3%).~~ The latter was a first indication that the

Formatted: Default Paragraph Font, English (United States)
Formatted: English (United States)
Formatted: English (United States)
Formatted: English (United States)
Formatted: English (United States)
Formatted: English (United States)
Formatted: English (United States)
Formatted: English (United States)
Formatted: English (United States)
Formatted: English (United States)
Formatted: English (United States)
Formatted: English (United Kingdom)

modified WCT method can~~could~~ detect the PBLH~~PBL top~~ efficiently, as long as the signal decrease threshold was tuned properly. The~~Hence, the PBL height could be identified in 53% of the cases with sufficient data availability (72 days). In Figure 2, the~~ data coverage is presented on a monthly basis in Figure 2. The highest PBLH~~PBL~~ detection frequency was achieved in February, which~~reaching 74%. This high detection rate~~ can be attributed to favorable meteorological conditions, since ~~in February the occurrence of~~ low clouds appeared sparsely without any~~was 0.7% with no~~ rainfall events.

~~3.2 Radiosonde measurements~~

The Bulk Richardson Number (BRN) method was used for PBL determination, employing the formula introduced by Menut et al. (1999):

$$Ri_b\,(h) = \frac{g(h-h_0)}{\theta(h)}\,\frac{[\theta(h)-\theta(h_0)]}{u(h)^2\,+\,\mathrm{v}\,(\mathrm{h})^2}$$

, where h is altitude, h_0 the altitude of the ground, g gravitational acceleration, θ potential temperature in Kelvin and u and v the zonal and meridional wind components, respectively. The PBL height was determined to be the lowest altitude where BRN reached the critical value, which is taken equal to 0.21 (Vogelezang 1996). Beyond this critical value of R_i, the atmosphere can be considered stable and fully decoupled from the underneath layer.

3.2~~3~~ Space-borne lidar observations

Cloud-Aerosol Lidar and Infrared Pathfinder Satellite Observation (CALIPSO) is an Earth Science observation mission that was launched on 28 April 2006. The vertical resolution of the CALIOP (Cloud-Aerosol Lidar with Orthogonal Polarization) system is 30 m. CALIPSO Level 2 aerosol layer product, provides a description of the aerosol layers, including their top and bottom height, identified by automated algorithms applied in the Level 1 data. Detailed description of the aforementioned algorithms can be found in Vaughan et al. (2004) and Winker (2006). In this study, CALIOP Version V4-10 dataset was used. Currently, no operational CALIOP PBL product is available.

More specifically~~In this study,~~ we applied the~~use~~ CALIOP Level 2 Aerosol Layer Product, which provides information on the base and top heights of existing aerosol layers, reported at a uniform 5 km horizontal resolution. Leventidou et al. (2013) evaluated the daytime PBLH~~PBL height~~ derived by Level 2 Aerosol Layer products over Thessaloniki, Greece, for a 5-year period, making the assumption that the lowest aerosol layer top can be considered as the PBLH~~PBL height~~. The aforementioned method was also applied over South Africa, revealing high agreement with ground based observations (Kohronen et al., 2014~~2013~~). During the measurement campaign, PBLH~~the PBL height~~ was ~~also~~ accessed by the space-borne lidar CALIOP, within ~~two~~ overpass distances of~~,~~ 20 and 101 km from Gual Pahari.

3.3 WRF~~4~~ Atmospheric Model~~model estimations~~

~~3.4.1~~ The **~~ECMWF model~~**

Formatted: Font color: Text 1, English (United States)

Formatted: Font color: Text 1, English (United States)

Formatted: English (United Kingdom)

Formatted: Font: Not Bold, English (United Kingdom)

~~The WRF~~ model, Version 3.9.1 (Skamarock et al., 2008) was also order to determine the PBLH~~PBL height~~. The simulation domain was the lidar station in Gual Pahari and three domains with a respective horizontal resolution of 18 km, 6 km and 2 km were used, where the two inner domains are two-way nested to their parent domain. The third inner-most domain covers an area between 75.84-78.46° E and 27.38-29.52°~~52 °~~ N. The output is provided every hour. On the vertical axis, 37 full sigma levels resolve the atmosphere up to 50 hPa (≈ 20 km AGL), with a finer grid spacing near the surface.

University scheme (YSU) (Hong et al., 2006) in conjunction with the land surface model Noah (Chen and Dundhia, 2001) was used for the estimation of PBL height. In addition, the Rapid Radiative Transfer Model (RRTM) scheme (Mlawer et al., 1997) for longwave radiation and the scheme of Dundhia (1989) for shortwave radiation were applied. A surface-layer scheme based on the revised MM5 similarity theory (Jimenez et al., 2012) as well as the Kain and Fritsch (1990, 1993) scheme for cumulus parameterization were used. For microphysics, the scheme proposed by Thompson et al. (2008) was considered. Regarding land use and soil types, the predefined datasets of Moderate Resolution Imaging Spectroradiometer (MODIS) with 21 land use classes were used. The initial and lateral boundary conditions were derived from the National Center for Environmental Prediction (NCEP) operational Global Fine Analysis (GFS) with 1 º x 1 º spatial resolution and were updated every 6 h. The Sea Surface Temperature (SST) was obtained from High Resolution Real-Time Global SST (RTG SST HR), with spatial resolution 0.083 º x 0.083 º which was renewed every 24 h.

In the YSU scheme, the top of the PBL ~~height~~ under unstable conditions is determined as the first neutral level based on the Bulk Richardson Number (Ri)~~BRN~~ calculated between the lowest model level and the levels above (Hong et al., 2006; Shin and Hong, 2011). Under stable conditions, the Ri~~BRN~~ is set as a constant value of 0.25 over land, enhancing mixing in the stable boundary layer (Hong and Kim 2008), whereas it is a function of the surface Rossby number over the oceans, following the study of Vickers and Mahrt (2003). More specifically, the revised Stable Boundary Layer (SBL) scheme (Hong 2010) computes the exchange coefficients with a parabolic function with height, as in the mixed layer, in which the top of the SBL is determined by the Ri (Vickers and Mahrt 2004). This leads to a gradual-and not abrupt-collapse of the mixed layer after the sunset, due to the residual superadiabatic layer near the surface even in the presence of negative surface buoyancy flux.

Within the frame of three case studies, the default simulated PBLH~~PBL height~~ from WRF was used to justify the lidar PBLH~~PBL heights. Furthermore, WRF profiles of temperature (T), relative humidity (RH) and potential temperature (θ) were compared to corresponding radiosonde profiles. The comparison was performed through specific criteria following the guidelines given by Seidel et al. (2010). In the T criterion, the base of an elevated temperature inversion is considered as the PBL top. Inversions do not appear in every profile, but when present, their base serves as a cap to the mixing processes below. In θ profiles, the level of the maximum vertical gradient (Oke, 1988; Stull, 1988; Sorbjan 1989; Garrat, 1992) was used, since this gradient is indicative of a transition from a~~

~~convectively less stable region below to a more stable region above. In a similar way, the level where~~

4 Results and Discussion~~discussion~~

4.1 Applicability of the WCT method: Case studies

It was found that in some cases the presence of multiple aerosol layers and low clouds can pose difficulties in PBLH detection (Section 3.1.3). However, these difficulties can be dealt with the use of proper WCT threshold and cut off values (Section 3.1.2). Three case studies of PBLH~~PBL~~ daily evolution were analyzed and evaluation with ancillary data sources was performed so as to investigate capabilities~~their strengths~~ and limitations~~limits~~. First, the evolution of PBLH~~PBL~~ under cloudless conditions is discussed for 12 February 2009. Subsequently, a two-day case with a multiple aerosol layer structure is presented for 1-2 March 2009. Finally, the diurnal development of PBLH~~PBL~~ is investigated in the presence of low clouds for 29 June 2008. ~~The three criteria (T_crit, RH_crit, θ_crit) were used to determine PBL height in each radiosonde profile. These criteria were also applied to WRF It was found that the presence of multiple aerosol layers and low clouds can pose difficulties in PBL top detection (Section 3.1.3). However, as it will be shown these difficulties can be dealt with the use of proper WCT threshold and cut off values (see Section 3.1.2).~~

The ~~diurnal evolution of~~ PBL during 12 February 2009 was characterized by an almost constant daily growth rate (133 m/h between 06:00 UTC and10:00 UTC) with a maximum height of 950 m (~~is presented in~~ Figure 3). ~~Sunrise was approximately at 01:30 UTC, while sunset was at 12:40 UTC.~~ No aerosol layers were observed in the free troposphere. Although~~found aloft. Between 06:00-12:00 UTC, although internal~~ gradients (yellow and red color) of aerosol content, appeared inside the PBL (06:00-12:00 UTC),~~,~~ the default signal decrease threshold (0.05) was efficient. However, later (~~Between~~ 12:00-18:00 UTC) in order to avoid strong gradients in the lower parts of the PBL, higher ~~a~~ threshold (~~of~~ 0.08) was used in conjunction with ~~a 90 m~~ cut-off heights (90 m). Furthermore, ~~height. Due to~~ low aerosol load conditions were responsible for high variability in~~content,~~ the derived PBLH (~~PBL heights between~~ 12:00-14:00 UTC). ~~showed high variability. An almost constant daily growth rate of 133 m/h was found from 06:00 UTC to 10:00 UTC. The maximum height of 950 m was reached at 10:30 UTC.~~

During convective hours (05:00-12:00 UTC), WRF overestimated the PBLH mainly due to the simulated neutral profile-virtual potential temperature at the surface similar to that around 1100 m AGL (differences < 0.5 K, not presented), resulting in an increase in the PBLH (Kim et al., 2013). It is worth mentioning that during the convective period FMI-Polly^{XT} identified a light aerosol load activity at the altitude where the numerical models estimated the PBLH, with the WCT technique not detecting this activity due to the weakness of the aerosol gradients. During night-time model estimations yielded lower PBLH compared to lidar data.. During night-time model estimations yielded lower PBLH compared to lidar data. The low wind field produced by the WRF close to the surface (wind speed values up to 3 m/s in the first kilometer) and, thus, the lack of sufficient mechanical turbulence, can be related to the shallow nocturnal PBL. It should be noted that the measured PBLH is expected to depict, apart from any mechanically-driven layer during the stable and transition periods, the top of the previous day's residual aerosol layer, while the simulated PBLH from WRF refers to the height of the

Formatted: English (United States)

shallow mixed layer. Therefore, their difference is expected since they depict different layers. The overall correlation was satisfying (r=0.8).

Figure 3 (middle panel) shows the development of PBL according to FMI Polly^{XT} measurements and the estimations from the two atmospheric models. During convective hours (05:00-12:00 UTC), the WRF and ECMWF models seemed to overestimate PBL height. On the other hand, during night-time model estimations yielded lower PBL heights compared to lidar data, since the former estimated the nocturnal PBL while the latter identified the RL top. Between 6:00 and 12:00 UTC, FMI Polly^{XT} identified a light aerosol load activity at the altitude where the WRF model estimated the PBL height. The correlation with lidar hourly heights was satisfying (r=0.8) for both model output data, while a

During the two- day period of 1-2 March 2009, a complex aerosol layer structure appeared in the free troposphere up to 3 km altitude (Figure 4). However, appropriate modification ofthe modified WCT method managed to detect the top of the PBL in most of the 15-min intervals, after modifying the signal decrease threshold and use of appropriate applying a cut-off heights allowed for the detection of PBLH. In order to avoid gradients in the lower parts of the PBL, the signalheight. The threshold was adjusted (within the range of 0.03-0.08) within , which corresponds to a 6-16% signal decrease, in combination withrespectively. Furthermore, a 30-60 m cut-off zoneheight was used, in order to avoid gradients in the lower parts of the PBL.

On 1 March 2009, the transition period (02:00- to 05:00 UTC) was characterized by a slow PBLHPBL development (of 14 m/h),, whereas the PBLHPBL evolution was more pronounced in the convective period (05:00- to 09:00 UTC) with a mean growth rate of 101 m/h. The maximum height (of 950 m) appeared at 08:45 UTC. On the next day, a stronger but slightly shorter PBLHPBL cycle was observed, with a mean evolution rate of 187 m/h, reaching a maximum height (of 1010 m) at 08:15 UTC15UTC. This slight modification in PBLHthe development of the PBL, can be attributed to the combination of higher temperature and lower wind speed conditions duringcharacterizing the second day.

4.1.3 Case with low clouds: 29 June 2008

In this case broken cumulus clouds appeared between 600-1100 m (from 00:00 to 12:00 UTC). On average, a moderate PBLH evolution (86 m/h) was found, with a maximum height (1279 m) appearing at 9:15 UTC (Figure 5). Whenever clouds appeared below 1km, we made the. The assumption that the cloud base isconstitutes an approach to the top approximation of the PBL, however top was made. However, it could be argued that the PBLHPBL top was located at a higher level, wheresince diffuse aerosol layers were found. In additionalso present there. During this period, it was difficult to findlocate an adequate signal decrease; the default gradient; a threshold corresponding to 10% decrease was used, while sensitivity tests with thresholds sensitive to weaker gradientslower threshold values yielded the same results. Hence, the algorithm exhibited decreased sensitivity, which can be attributed is mainly related to the existence of diffuse aerosol layers. High PBLH was observed immediately after, due to

Large PBL height values also appeared around 12:00 UTC, corresponding to a strong aerosol layer which sprawled to lower heights, either through probably due to dry removal or precipitation that

Formatted: English (United Kingdom)

evaporated before reaching the ground. Following a short ~~Rainfall was observed between 13:30 and~~ remaining aerosol~~aerosols~~ kept being displaced downwards~~in the downward direction~~, creating strong the ~~The effect of~~ aerosol removal effect was clear (~~can be seen between~~ 16:00~~ and~~ 24:00 UTC) aerosol load~~, observed, complicated~~ the detection of PBLH was complicated and, hence, accounted~~the~~ PBLH (~~the detected PBL heights between~~ 16:00~~ and~~ 24:00 UTC)~~.~~ .

WRF ~~and ECMWF estimations~~ correlated well with FMI-Polly^{XT} ~~hourly PBL height data~~ (r=0.74)~~. and r=0.69, respectively).~~ During daytime, WRF slightly overestimated PBLH~~PBL height~~, while it should be noted that FMI-Polly^{XT} identified intermittent aerosol gradients at~~an underestimation was observed during night-time by both models. Good agreement was corroborated by additional statistical parameters. Fractional bias was equal to 0.015 and 0.11 for WRF and ECMWF estimations, respectively.~~

4.2 Comparison ~~of lidar PBL heights to ancillary data sources~~

During the measurement period, 24 CALIPSO overpasses were available within~~inside~~ 1° radius around Gual Pahari station. The Boundary Top Location~~In 17 cases the boundary top location~~ algorithm (~~SIBYL (,~~ Selective Iterated Boundary Locator) identified two to four layers (17 cases), while~~, whilst~~ in the remaining~~7~~ cases no layers were identified. However, ~~For the 17 cases, the PBL top from the~~ ground-based lidar observations were not ~~was~~ available in all ~~for 14 cases. In one case, the top~~ of the cases (only in 14)~~.second layer was chosen, as the first one was inside the PBL, according to the attenuated backscatter image from CALIOP.~~ Furthermore, some~~5~~ cases (5) were excluded from~~not included in~~ the comparison as the detected layers were clearly~~either~~ above the typical PBL limits (higher than ~~(height >~~3 km)~~.) or in the free troposphere (height >10 km).~~

4.3 Statistical Analysis

4.3.1 ~~PBL~~ Diurnal Cycle of PBLH

~~Figure 8a shows the mean diurnal PBL evolution as obtained by lidar measurements and ECMWF estimations.~~ Although night-time PBLH is~~PBL height values were~~ not taken into account for the statistical analysis of ~~PBL~~ seasonal PBLH (Section 4.4.2)~~, height,~~ nocturnal PBLH is considered~~values are included~~ here in order~~so as~~ to investigate~~present~~ the ~~PBL~~ diurnal ~~evolution.~~

~~ECMWF estimations revealed a shorter but stronger PBL growth period, with a maximum top height of 2137 ± 143 m, which appeared earlier than the one given by FMI-Polly^{XT}. As in the annual and winter diurnal cycle, ECMWF overestimated PBL top height during convective hours. On the other hand, underestimation was observed during the early morning hours, with a more significant underestimation during night-time due to the fact that FMI-Polly^{XT} identified the RL, whereas the ECMWF estimated the nocturnal PBL top. The total comparison reached an r of 0.84.~~

In this Section~~the following,~~ we statistically analyze~~present the main statistical findings regarding~~ the lidar measurements in conjunction with the~~during 72 days. The~~ seasonal cycle of mean and maximum seasonal mean PBLH~~PBL height~~ was found at 695 ± 146 m during winter~~, (17 days),~~ 878 ± 297 m period ~~(15 days)~~ and 1025 ± 296 m during the monsoon. The ~~(40 days). Regarding the~~ seasonal

at 1191 ± 516 m during winter, 1326 ± 565 m during the pre-monsoon period and at 1361 ± 350 m during the monsoon. In general, the PBLH seasonal cycle followed the temperature cycle very well. The temperature cycle of the ~~During the~~ measurement days was fairly representative of the whole seasonal cycle, with the temperature distribution being similar to the distributions of the whole seasonal periods. During the measuring period, a mean temperature of 21 ± 4 ºC was found in ~~the~~ winter, 27 ± 3 in the pre-monsoon and 30 ± 2 ºC in the monsoon season while the~~.~~ ~~A~~ seasonal average maximum temperature ~~of 29 ± 5 ºC~~ was recorded at 29 ± 5 ºC~~in the winter~~, 33 ± 4 ºC ~~in the pre-monsoon~~ and 35 ± 2 ºC accordingly. Nevertheless, it should be mentioned that~~in the monsoon period.~~

In winter, the daily mean PBLH distribution was narrower (in majority between 600 and 900 m) compared to the pre-monsoon and monsoon seasons (mostly between 900 and 1200 m). Following a similar pattern, the daily maximum PBLH was rather confined in winter (in majority between 900 and 1200 m) with a significantly broader spectrum (between 600 and 1800 m) in pre-monsoon and monsoon. The highest inter-seasonal variability was exhibited during ~~the~~ pre-monsoon ~~season both in terms of mean and maximum PBL height~~, which could~~may~~ be attributed to ~~the~~ meteorological conditions. The ~~of this period. During the~~ pre-monsoon season comprised days~~, 7 cases~~ with heavy rainfall and days~~(7 37 mm daily accumulated precipitation) and 8 cases~~ with hardly any precipitation, which can potentially explain the ~~appeared (less than 3 mm accumulated precipitation). This combination led to a~~ broad distribution of daily mean PBLH (~~PBL heights (from~~ 251~~- m to~~ 1191 m). In winter large ~~Large~~ inter-seasonal variability ~~was also observed in the winter period, in terms~~ of attributed to the broad inter-seasonal ~~range of maximum~~ temperature range ~~, which was almost 16 ºC~~ (20 ºC - 36 ºC).

~~The frequency distribution of daily mean PBL height is presented in Figure 9 for 6 different classes of 300 m. During the measurement campaign, the majority of daily mean PBL heights were found between the classes of 600 and 1200 m (40% within 600-900 m; 32% within 900-1200 m). The winter period distribution was narrower and skewed towards the 600-900 m class. In the pre-monsoon and monsoon seasons, PBL height distributions were quite broader with a maximum between 900 and 1200 m. In terms of daily maximum PBL height, the majority of heights were found between 900 and 1800 m (26% within 900-1200 m; 22% within 1200-1500 m; 29% within 1500-1800 m). In the winter period, a more confined distribution appeared, with 53% of daily maximum heights between 900 and 1200 m. The PBL height spectrum was significantly broader in the pre-monsoon and monsoon periods, with maximum daily heights to spread between 600 and 1800 m.~~

During the~~The distribution of daily growth rates is presented in Figure 9. For the whole~~ measurement period, daily evolution rates were mostly within ~~observed in the~~ 100-200 m/h but lower rates (~~class, while a significant number of mean growth rates was observed between~~ 29-100 m/h) ~~, Different frequency distributions~~ were observed as well. In winter~~on each seasonal period, albeit the average evolution rates did not exhibit strong seasonal variability. In the winter period~~, daily growth rates presented a slightly broad distribution ~~(mostly with most of them lying~~ between 100 and 200 m/h) with ~~(40%), while~~ a mean evolution ~~rate~~ of 157 ± 81 m/h (Figure 8)~~.N=15) was found.~~ In ~~the~~ pre-monsoon, slightly ~~season,~~ higher growth rates were observed (mainly within 100-300 m/h), with an average of , 206 ± 134 m/h. Additionally, rates between 0-100 m/h and 500-600 m/h ~~(N=9), with 44% of them~~

Formatted: English (United States)
Formatted: English (United States)
Formatted: English (United States)
Formatted: English (United States)
Formatted: English (United States)
Formatted: English (United States)
Formatted: English (United States)
Formatted: English (United States)
Formatted: English (United States)
Formatted: English (United States)
Formatted: English (United States)
Formatted: English (United States)

~~within the range 100-200 m/h, while 33%~~ were observed, following the pattern of ~~between 200 and 300~~ pre-monsoon season (Section 4.4.2).~~.~~ In the monsoon~~, season, lower~~ evolution speeds were slightly lower ~~observed~~ (121 ± 67 m/h) ~~, N=22), with 45% being less than 100 m/h., while a significant~~ ~~percentage (40%) was found between 100 and 200 m/h.~~

~~The average PBL height was lower in Gual Pahari (866 m) in comparison to Elandsfontein (1400 m) with less seasonal variability (standard deviation of 165 m in Gual Pahari; 500 m in Elandsfontein). In both sites the maximum PBL height was reached approximately three hours after the solar noon, since the daily solar cycle is similar in the latitudes of the two stations. In Gual Pahari, the highest rates (mostly within 100-300 m/h) appeared in the pre-monsoon season (April-May), whilst in Elandsfontein~~ maximum rates (between 120-320 m/h) were reached during spring~~. (~~September-October, (Kohronen et al., 2014) a period that exhibits strong similarities with the ~~). The~~ pre-monsoon season in India~~. and the spring season in South Africa have strong similarities.~~

~~5~~6 Summary and Conclusions

In this study~~paper~~, one year long ground-based lidar measurements were used to retrieve PBLH~~analyze PBL height variability~~ over Gual Pahari, New Delhi. The feasibility of deriving PBLH with the modified WCT technique was investigated and the respective results~~lidar retrieved PBL heights~~ were compared to ~~data from~~ independent sources.

In~~: radiosondes, satellite observations and two atmospheric models. Three case studies of PBL daily evolution were discussed so as to identify atmospheric structures which can complicate PBL height detection. It was found, in~~ support of previous work (Baars et al., 2008; Korhonen et al., 2014), it was found~~2013),~~ that the modified WCT method exhibited satisfying efficiency ~~performed well~~ under different meteorological and aerosol load regimes. On a case with elevated aerosol layers,~~More specifically, a~~ significantly good performance was revealed, even when the layers were injected into the PBL. Such layers have been reported in literature as ~~on~~ a major challenge in the attribution of the PBLH especially during night-time (Haeffelin et al., 2012). PBLH~~two day case, with multiple aerosol layers aloft. However, PBL~~ determination was complicated in the presence of ~~before a rain event, where lofted layers created strong aerosol content gradients and later on, where~~ diffuse aerosol layers. Low aerosol load, observed mainly during morning or afternoon transitions, also represents a condition for uncertain determination of PBLH (Haeffelin et al., 2012). Sensitivity analysis revealed stable performance of the WCT algorithm, with the exception of elevated layers and PBL internal gradients, which affected the results when specific thresholds were applied. Higher thresholds appeared to be more sensitive towards detecting lofted layers.

In the context of the aforementioned cases, WRF model ~~case studies, numerical estimations~~ overestimated PBLH~~PBL height~~ in the daytime, while an underestimation was observed in the night-time. The understanding of turbulence in nocturnal SBL and its parameterization is rather slow and not well established in NWP models (Mahrt et al., 1999; Beare et al., 2006; Hong 2010). In this study, this

Formatted: English (United States)
Formatted: English (United States)
Formatted: English (United States)
Formatted: List Paragraph, Justified, Line spacing: 1.5 lines
Formatted: Font: Times New Roman, 10 pt, English (United States)
Formatted: Font: Times New Roman, 10 pt, English (United States)
Formatted: Font: Times New Roman, 10 pt, English (United States)
Formatted: Font: 10 pt, English (United States)

is ~~The latter can be~~ partly addressed by the revised SBL scheme that retains the turbulent levels so as to avoid the abrupt collapse of the mixed layer after the sunset by using the exchange coefficients.~~attributed to the fact that the lidar system identified the RL, whereas the numerical models estimated the nocturnal PBL top. The comparison between radiosonde and WRF vertical profiles, through three different methods, showed that radiosonde data overestimated PBL height in the night-time. The discrepancies between radiosonde and WRF PBL heights could be attributed to various sources, such as the different vertical resolution and the different nature of each data set; radiosondes provide in situ measurements, whereas WRF model provides numerical estimations of various meteorological parameters.~~ However, the fact that neither anthropogenic heat sources nor heat storage in buildings were~~are~~ included in the simulations could also explain the model underestimation. Furthermore, it should be noted that the measurements often depict different layers from the simulated ones, as in the case of the residual aerosol layer.

During the rainy season of monsoon, the diurnal cycle of PBLH was weaker and its evolution was completed earlier. A relatively warmer and drier winter and, respectively, a colder and rainier pre-monsoon were observed compared to climatological records. These meteorological patterns could account for the observed PBLH cycle, which was rather indistinct compared to the cycle expected from long-term climate statistics. Daily evolution rates of 29-200 m/h were mainly observed, with lower rates during the rainy season of monsoon.~~The evolution of PBL started two to four hours after sunrise and was completed two hours after the solar noon, with the maximum PBL height observed approximately one hour later. In the winter and pre-monsoon season, ECMWF data revealed a stronger PBL daily evolution. During the monsoon season, both FMI-Polly^{XT} measurements and ECMWF output data, produced a smoother diurnal cycle, consisting of weaker fluctuations between daytime and night time, with PBL heights from ECMWF being systematically lower than those derived from FMI-~~ Future studies are necessary in order to better understand the factors that modulate the exchange of moisture, heat and momentum between the surface and PBL and, consequently, affect the comparison of modelled PBLH with observational data. In addition, the relative contribution of the various PBL dynamics drivers, under different aerosol load and meteorological regimes, needs to be further investigated. The feasibility of applying the modified WCT method in simpler lidar systems such as ceilometer and Doppler lidar, should be assessed. These systems entail less operational cost and, thus, exhibit good potential for determining the PBLH and evaluating weather prediction and pollution dispersion models on an operational basis. In recent years, significant effort has been made towards the establishment of ceilometer networks by national weather services and other agencies over Europe with the aim to build up a framework for real-time applications and improvements of air quality and weather prediction by assimilation of ceilometer data (Haeffelin et al., 2012; Wiegner et al., 2014). Analogous efforts are currently in progress over different parts of India, like in the states of Maharashtra and Kerala and in the union territory of Delhi (Sharma et al., 2016; Babu et al., 2017; https://www.lufft.com/projects/several-lufft-chm-15k-ceilometer-projects-in-india-529/). ~~The seasonal PBL cycle observed during the measurement campaign was less pronounced than the one expected from climatological records. This could be attributed to the combination of a relatively warmer winter and a colder pre-monsoon period with respect to long-term climate statistics. The highest values of~~

Formatted: English (United States)

Formatted: English (United States)

~~mean and maximum PBL height appeared in the monsoon season, where the highest mean and~~

Appendix A: Sensitivity Analysis of the WCT threshold

In cases of elevated layers or aerosol gradients within the PBL, it has been revealed that the signal decrease threshold needs to be properly adjusted (Section 4.1). In this study, we adapted the threshold (t) so that the WCT algorithm was allowed to identify signal gradients in the order of 6-16% (t=0.03-0.08, correspondingly). In this Section, we investigate the effect of the WCT threshold on the estimated PBLH. For this reason, we performed a sensitivity analysis modifying the signal decrease threshold for the case of 2 March 2009, where elevated layers were injected into the PBL.

The overall performance of the WCT technique was stable (Figure 9), with the threshold affecting the results in only a few cases. When the lowest and more sensitive to detect weak layers threshold (0.03) was applied, a thin aerosol layer (around 1300 m) was identified (see Figure 4). At this time (07:00 UTC), increased thresholds (0.04-0.08) detected a stronger elevated layer (approximately at 2 km). The lowest threshold was also more efficient when gradients appeared inside the PBL (around 17:00 UTC), with the higher thresholds yielding increased PBLH by approximately 300 m. When the elevated layers were characterized by higher aerosol load (18:00-19:00 UTC), lower thresholds (0.03-0.05) performed better as well, with the higher ones identifying stronger layers (around 1 km). Thus, the PBLH deviation, introduced by the modification of the WCT threshold, appeared to depend on the altitude of internal gradients or elevated layers. However, in the early morning (00:00-03:00 UTC), where the convective activity was not initiated yet, a minor fluctuation (30 m) was observed, related to the algorithm's sensitivity towards aerosol content gradients.

An adequate threshold adaptation also affected the agreement with the modelled PBLH. More specifically, it is shown (Figure 9) that during cases where the applied threshold induced a deviation from the smooth PBLH evolution, the disagreement with modelled PBLH increased as well. Besides, the agreement with the simulated PBLH appears to depend on the altitude of the atmospheric features (internal or elevated aerosol gradients) that affect the performance of the WCT algorithm.

Appendix B: ~~,~~ Statistical Indicators~~parameters formulas~~

Formatted: Font: Bold

~~Mean Normalized Bias~~

$$R = \frac{\sum_{i=1}^{N}(O_i - \overline{O}) \cdot (M_i - \overline{\overline{M}})}{\sqrt{\sum_{i=1}^{N}(O_i - \overline{O})^2} \cdot \sqrt{\sum_{i=1}^{N}(M_i - \overline{M})^2}}$$

M_i denotes predicted values from models, while O_i stands for observations at i, respectively. N is the number of samples.

Acknowledgements

This work (the campaigns) was partly funded by the European Integrated project on Aerosol Cloud Climate and Air Quality Interactions, EUCAARI. This work was supported by the Cy-Tera Project

(NEA YPODOMH/STRATH/0308/31), which is co-funded by the European Regional Development Fund and the Republic of Cyprus through the Research Promotion Foundation.

References

Althausen, D., Engelmann, R., Baars, H., Heese, B., Ansmann, A., Müller, D., Komppula, M.: Portable Raman Lidar Polly XT for Automated Profiling of Aerosol Backscatter, Extinction, and Depolarization. Journal of Atmospheric and Oceanic Technology 26, 2366–2378. https://doi.org/10.1175/2009JTECHA1304.1, 2009.

Amiridis, V., Melas, D., Balis, D.S., Papayannis, A., Founda, D., Katragkou, E., Giannakaki, E., Mamouri, R.E., Gerasopoulos, E., Zerefos, C.: Aerosol Lidar observations and model calculations of the Planetary Boundary Layer evolution over Greece, during the March 2006 Total Solar Eclipse. Atmospheric Chemistry and Physics 7, 6181–6189, 2007.

Ansmann, A., Riebesell, M., and Weitkamp, C.: Measurements of aerosol profiles with Raman lidar, Opt. Lett., 15, 746–748, 1990.

Ansmann, A., Wandinger, U., Riebesell, M., Weitkamp, C., and Michaelis, W.: Independent measurements of extinction and backscatter profiles in Cirrus clouds by using a combined Raman elastic-backscatter Lidar, Appl. Optics, 31, 7113–7131, 1992

Babu, S., Kumar, A., Padmalal, D., Nair, S., Resmi, E.A., Sorcar, N., Raj, S.R., Rejani R.P.: Annual Report 2017-2018. ESSO-National Centre for Earth Science Studies, Ministry of Earth Sciences, Government of India.

Baars, H., Ansmann, A., Engelmann, R., Althausen, D.: Continuous monitoring of the boundary-layer top with lidar. Atmospheric chemistry and Physics 8, 7281–7296, 2008.

~~Beljaars, A. C. M.: The impact of some aspects of the boundary layer scheme in the ECMWF model. In Proc. of ECMWF Seminar on Parameterization of Sub-grid Scale Physical Processes, pp. 125{161, Reading, 5{9 September 1994, 1995.~~

Beare R.J., Macvean M.K., Holtslag A.A.M., Cuxart J., Esau I., Golaz J.C., Jimenez M.A., Khairoutdinov M., Kosovic B., Lewellen D., Lund T.S., Lundquist J.K., McCabe A., Moene A.F., Noh Y., Raasch S., Sullivan P.: An intercomparison of large-eddy simulations of the stable boundary layer. Boundary-Layer Meteorol. 118: 247–272, 2006.

Binietoglou, I., Amodeo, A., D'Amico, G., Giunta, A., Madonna, F., and Pappalardo, G.: Examination of possible synergy between lidar and ceilometer for the monitoring of atmospheric aerosols, Proc. SPIE 8182, Lidar Technologies, Techniques, and Measurements for Atmospheric Remote Sensing VII, SPIE 8182, 818209, doi:10.1117/12.897530, 2011.

Boers, R., Eloranta, E.W.: Lidar measurements of the atmospheric entrainment zone and the potential temperature jump across the top of the mixed layer. Boundary-Layer Meteorology 34, 357–375, 1986.

Bravo-Aranda, J. A., de Arruda-Moreira, G., Navas-Guzmán, F., Granados-Muñoz, M. J., Guerrero-Rascado, J. L., Pozo-Vázquez, D.,Arbizu-Barrena, C., Olmo, F. J., Mallet, M., and Alados-Arboledas, L.: PBL height estimation based on lidar depolarisation measurements (POLARIS), Atmospheric Chemistry and Physics Discussions, 2016, 1–24, https://doi.org/10.5194/acp-2016-718, 2016.

Brooks, I.M.: Finding boundary layer top: Application of a wavelet covariance transform to lidar backscatter profiles. Journal of Atmospheric and Oceanic Technology 20, 1092–1105, 2003.

Chen, F., Dudhia, J.: Coupling an advanced land surface–hydrology model with the Penn State–NCAR MM5 modeling system. Part I: Model implementation and sensitivity. Monthly Weather Review 129, 569–585, 2001.

Cimini, D., De Angelis, F., Dupont, J.-C., Pal, S., Haeffelin, M.: Mixing layer height retrievals by multichannel microwave radiometer observations. Atmospheric Measurement Techniques 6, 2941–

Formatted: Font color: Auto

Formatted: Justified

2951. https://doi.org/10.5194/amt-6-2941-2013, 2013.

Cohn, S. A. and Angevine, W. M.: Boundary layer height and entrainment zone thickness measured by lidars and wind-profiling radars, J. Appl. Meteorol., 39, 1233–1247, 2000.

Davis, K.J., Gamage, N., Hagelberg, C.R., Kiemle, C., Lenschow, D.H., Sullivan, P.P.: An objective method for deriving atmospheric structure from airborne lidar observations. Journal of Atmospheric and Oceanic Technology 17, 1455–1468, 2000.

de Arruda Moreira, G. and Guerrero-Rascado, J. L. and Benavent-Oltra, J. A. and Ortiz-Amezcua, P. and Rom\'an, R. and Esteban Bedoya-Vel\'asquez, A. and Bravo-Aranda, J. A. and Olmo-Reyes, F. J. and Landulfo, E. and Alados-Arboledas, L.: Analyzing the turbulence in the Planetary Boundary Layer by the synergic use of remote sensing systems: Doppler wind lidar and aerosol elastic lidar. Atmos. Environ., 213, 185-195~~Atmospheric Chemistry and Physics Discussions, 1-24, 10.5194/acp-2018-276~~, 2018.

Dudhia J.: Numerical Study of Convection Observed during the Winter Monsoon Experiment Using a Mesoscale Two-Dimensional Model, J. Atmos. Sci., 46, 3077-3107, 1989.

Engelmann, R., Wandinger, U., Ansmann, A., M¨uller, D., Zeromskis,E., Althausen, D., and Wehner, B.: Lidar observations of the vertical aerosol flux in the planetary boundary layer, J. Atmos.Ocean. Tech., 25, 1296–1306, 2008.

Engelmann, R. and Kanitz, T. and Baars, H. and Heese, B. and Althausen, D. and Skupin, A. and Wandinger, U. and Komppula, M. and Stachlewska, I. S. and Amiridis, V. and Marinou, E. and Mattis, I. and Linn\'e, H. and Ansmann, A.: The automated multiwavelength Raman polarization and water-vapor lidar Polly^{XT}: the neXT generation. Atmospheric Measurement Techniques. 4, 1767-1784 10.5194/amt-9-1767-2016, 2016.

Garratt, J. R.: The Atmospheric Boundary Layer, 335 pp., Cambridge Atmospheric and Space Science Series, Cambridge Univ. Press, 1992.

Groß, S., Gasteiger, J., Freudenthaler, V., Wiegner, M., Geiß, A., Schladitz, A., Toledano, C., Kandler, K., Tesche, M., Ansmann, A. and Wiedensohler, A.: Characterization of the planetary boundary layer during SAMUM-2 by means of lidar measurements. Tellus 63B, 695–705, doi:10.1111/j.1600-0889.2011.00557.x, 2011.

Haeffelin, M., Angelini, F., Morille, Y., Martucci, G., Frey, S., Gobbi, G.P., Lolli, S., O'Dowd, C.D., Sauvage, L., Xueref-Rémy, I., Wastine, B., Feist, D.G.:Evaluation of Mixing-Height Retrievals from Automatic Profiling Lidars and Ceilometers in View of Future Integrated Networks in Europe. Boundary-Layer Meteorology 143, 49–75. https://doi.org/10.1007/s10546-011-9643-z, 2012.

Hegde, P., Pant, P., Naja, M., Dumka, U. C., and Sagar, R.: South Asian dust episode in June 2006: Aerosol observations in the central Himalayas, Geophys. Res. Lett., 34, L23802, doi:10.1029/2007GL030692, 2007.

Hong, S.-Y., Noh, Y., Dudhia, J.: A new vertical diffusion package with an explicit treatment of entrainment processes. Monthly weather review 134, 2318–2341, 2006.

Hong, S.-Y., Kim, S.-W.: Stable boundary layer mixing in a vertical diffusion scheme. Proc. Ninth Annual WRF User's Workshop, Boulder, CO, National Center for Atmospheric Research, 3.3. [Available online at http://www.mmm.ucar.edu/ wrf/users/workshops/WS2008/abstracts/3-03.pdf., 2008

Hong S.-Y.: A new stable boundary-layer mixing scheme and its impact on the simulated East Asian summermonsoon. Q. J. R. Meteorol. Soc. 136: 1481–1496, 2010.

Hyvärinen, A.-P., Lihavainen, H., Komppula, M., Panwar, T.S., Sharma, V.P., Hooda, R.K., Viisanen,

Y.: Aerosol measurements at the Gual Pahari EUCAARI station: preliminary results from in-situ measurements. Atmospheric Chemistry and Physics 10, 7241–7252, 2010.

Hyvärinen, A.-P., Raatikainen, T., Komppula, M., Mielonen, T., Sundström, A.-M., Brus, D., Panwar, T.S., Hooda, R.K., Sharma, V.P., de Leeuw, G., Lihavainen, H.: Effect of the summer monsoon on aerosols at two measurement stations in Northern India – Part 2: Physical and optical properties. Atmospheric Chemistry and Physics 11, 8283–8294. https://doi.org/10.5194/acp-11-8283-2011, 2011.

Jiménez, P.A., Dudhia, J., González-Rouco, J.F., Navarro, J., Montávez, J.P., García-Bustamante, E.: A Revised Scheme for the WRF Surface Layer Formulation. Monthly Weather Review 140, 898–918. https://doi.org/10.1175/MWR-D-11-00056.1, 2012.

Jordan, N.S., Hoff, R.M., Bacmeister, J.T.: Validation of Goddard Earth Observing System-version 5 MERRA planetary boundary layer heights using CALIPSO: VALIDATION OF GEOS-5 USING CALIPSO. Journal of Geophysical Research: Atmospheres 115. https://doi.org/10.1029/2009JD013777, 2010.

Kain, J. S. and Fritsch, J. M.: A one-dimensional entraining/ detraining plume model and its application in convective parameterization, J. Atmos. Sci., 47, 2784-2802, 1990.

Kain, J. S. and Fritsch, J. M.: Convective parameterization for mesoscale models: The Kain-Fritcsh scheme. The representation of cumulus convection in numerical models, K. A. Emanuel and D.J. Raymond, Eds., Amer. Meteor. Soc., 246 pp, 1993.

Kim, Y., Sartelet, K., Raut, J.-C., Chazette P.: Evaluation of the Weather Research and Forecast/Urban Model Over Greater Paris, Boundary-Layer Meteorology, 149(1), 105–132. https://doi.org/10.1007/s10546-013-9838-6, 2013.

Klett, J. D.: Stable analytical inversion solution for processing lidar returns, Appl. Optics, 20, 211–220, 1981.

Klett, J. D.: Lidar inversions with variable backscatter/extinction velues, Appl. Optics, 24, 211–220, 1985.

Komppula, M., Mielonen, T., Arola, A., Korhonen, K., Lihavainen, H., Hyvärinen, A.-P., Baars, H., Engelmann, R., Althausen, D., Ansmann, A., Müller, D., Panwar, T.S., Hooda, R.K., Sharma, V.P., Kerminen, V.-M., Lehtinen, K.E.J., Viisanen, Y.: Technical Note: One year of Raman-lidar measurements in Gual Pahari EUCAARI site close to New Delhi in India – Seasonal characteristics of the aerosol vertical structure. Atmospheric Chemistry and Physics 12, 4513–4524. https://doi.org/10.5194/acp-12-4513-2012, 2012.

Korhonen, K., Giannakaki, E., Mielonen, T., Pfüller, A., Laakso, L., Vakkari, V., Baars, H., Engelmann, R., Beukes, J.P., Van Zyl, P.G., Ramandh, A., Ntsangwane, L., Josipovic, M., Tiitta, P., Fourie, G., Ngwana, I., Chiloane, K., Komppula, M.: Atmospheric boundary layer top height in South Africa: measurements with lidar and radiosonde compared to three atmospheric models. Atmospheric Chemistry and Physics 14, 4263–4278. https://doi.org/10.5194/acp-14-4263-2014, 2014.

Kulmala, M., Asmi, A., Lappalainen, H. K., Baltensperger, U.,Brenguier, J.-L., Facchini, M. C., Hansson, H.-C., Hov, Ø.,O'Dowd, C. D., P¨oschl, U., Wiedensohler, A., Boers, R.,Boucher, O., de Leeuw, G., Denier van den Gon, H., Feichter,J., Krejci, R., Laj, P., Lihavainen, H., Lohmann, U., McFiggans,G., Mentel, T., Pilinis, C., Riipinen, I., Schulz, M., Stohl, A.,Swietlicki, E., Vignati, E., Amann, M., Ammann, M., General overview: EuropeanIntegrated project on Aerosol Cloud Climate and Air Qualityinteractions (EUCAARI) – integrating aerosol research from nano to global scales, Atmos. Chem. Phys., 11, 13061–13143,doi:10.5194/acp-11-13061-2011, 2011.

Lammert, A., Bösenberg, J.: Determination of the convective boundary-layer height with laser remote sensing. Boundary-Layer Meteorology 119, 159–170. https://doi.org/10.1007/s10546-005-9020-x, 2006.

Formatted: Font color: Auto

Lange, D., et al., 2014: Atmospheric boundary layer height monitoring using a Kalman filter and backscatter lidar returns, IEEE Transactions on *Geos. Rem. Sensing*, **52**, 4717-4728, doi:10.1109/TGRS.2013.2284110.

Lau W.KM, Kim K.M., Hsu C.N. Possible influences of air pollution, dust- and sandstorms on the Indian monsoon. WMO Bulletin 58 (1)-January 2009.Lelieveld, J., Crutzen, P. J., Ramanathan, V., Andreae, M. O., Brenninkmeijer,C. A. M., Campos, T., Cass, G. R., Dickerson, R. R.,Fischer, H., de Gouw, J. A., Hansel, A.,, Jefferson, A., Kley, D.,de Laat, A. T. J., Lal, S., Lawrence, M. G., Lobert, J. M., Mayol-Bracero, O. L., Mitra, A. P., Novakov, T., Oltmans, S. J., Prather,K. A., Reiner, T., Rodhe, H., Scheeren, H. A., Sikka, D., andWilliams, J.: The Indian Ocean Experiment: Widespread air pollution from South and Southeast Asia, Science, 291, 1031–1036,2001.

Leventidou, E., Zanis, P., Balis, D., Giannakaki, E., Pytharoulis, I., Amiridis, V.: Factors affecting the comparisons of planetary boundary layer height retrievals from CALIPSO, ECMWF and radiosondes over Thessaloniki, Greece. Atmospheric environment 74, 360–366., 2013.

~~Louis, J. F.,~~ Mahrt L., Sun J., Blumen W., Delany T., Oncley S.: Nocturnal boundary-layer regimes. Boundary-Layer Meteorol. 88: 255–278,1999.

~~Tiedtke, M. and Geleyn, J. F. (1982). A short history of the operational PBL~~

Melfi, S.H., Spinhirne, J.D., Chou, S.H., Palm, S.P.; Lidar observation of the vertically organized convection in the planetary boundary layer over the ocean.J. Clim. Appl. Meteorol. 24, 806e821, 1985.

Mlawer E. J., Taubman S. J., Brown P. D., Iacono M. J. and Clough S. A.: Radiative transfer for inhomogeneous atmospheres: RRTM, a validated correlated-k model for the longwave, J. Geophys. Res., 102 (D14), 16663-16682, 1997.

Morille, Y., Haeffelin, M., Drobinski, P., and Pelon, J.: STRAT: an automated algorithm to retrieve the vertical structure of the atmospherefrom single–channel lidar data, J. Atmos. Ocean. Tech., 24, 761–775, 2007.

Münkel, C.: Mixing height determination with lidar ceilometers–results from Helsinki testbed, Meteorol. Z., 16, 451–459, doi:10.1127/0941-2948/2007/0221, 2007.

Nakajima, T., Yoon, S.-C., Ramanathan, V., Shi, G.-Y., Takemura,T., Higurashi, A., Takamura, T.Aoki,K.,Sohn,B.J.,Kim, S.-W., Tsuruta, H., Sugimoto, N., Shimizu, A. Tanimoto, H., Sawa, Y., Lin, N.-H., Lee, C.-T., Goto, D., and Schutgens,N.: Overview of the atmospheric Brown Cloud East Asian Regional Experiment 2005 and a study of the aerosol direct radiative forcing in east Asia, J. Geophys. Res., 112, D24S91, doi:10.1029/2007JD009009, 2007.

~~Nieuwstadt, F. T. M.: The turbulent structure of the stable, nocturnal boundary layer. J. Atmos. Sci., 41, 2202–2216, 1984.~~

Nakoudi K., Giannakaki E., Baars H., Amiridis V., Tombrou M., Komppula M. "Planetary Boundary Layer variability over New Delhi, India during EUCAARI project", EGU General Assembly, Vienna, Austria, 8-13 April 2018,Vol. 20, EGU2018-809, 2018.

Oke, T. R.: Boundary Layer Climates, 2nd ed., 435 pp., Halsted Press, New York, 1988.

Palm, S.P., Hagan, D., Schwemmer, G., Melfi, S.H.: Inference of marine atmospheric boundary layer moisture and temperature structure using airborne lidar and infrared radiometer data. J. Appl. Meteorol. 37, 308e324. CrossRef, Web of Science_ Times Cited: 7, ADS, 1998.

Palm, S.P., Benedetti, A., Spinhirne, J.: Validation of ECMWF global forecast model parameters using GLAS atmospheric channel measurements. Geophys. Res. Lett. 32, 2005.

Perrino, C., Tiwari, S., Catrambone, M., Torre, D.D., Rantica, E., Canepari, S.: Chemical characterization of atmospheric PM in Delhi, India, during different periods of the year, including Diwali festival. Atmos Pollut. Res. 2, 418–427,2011.

Formatted: English (United Kingdom)

Formatted

Formatted: English (United States)

Formatted

Formatted: English (United States)

Formatted

Formatted: Normal, Left, Right: 0", Don't adjust space between Latin and Asian text, Don't adjust space between Asian text and numbers

Formatted: English (United Kingdom)

Pielke, R. A., Davey, C. A., Niyogi, D., Fall, S., Steinweg-Woods, J., Hubbard, K., Lin, X., Cai, M., Lim, Y. K., and Li, H.: Unresolved issues with the assessment of multidecadal global land surface temperature trends, J. Geophys. Res., 112, D16113, doi:10.1029/2006JD008229, 2007.

Ramanathan, V., Li, F., Ramana, M. V., Praveen, P. S., Kim, D., Corrigan, C. E., Nguyen, H., Stone, E. A., Schauer, J. J., Carmichael, G. R., Adhikary, B., and Yoon, S. C.: Atmospheric brown clouds: Hemispherical and regional variations in longrange transport, absorption, and radiative forcing, J. Geophys. Res., 112, D22S21, doi:10.1029/2006JD008124, 2007a.

Reddy, M. S. and Venkataraman, C.: Inventory of aerosol and sulphur dioxide emissions from India: I—Fossil fuel combustion,Atmos. Environ., 36, 677–697, 2002a.

Reddy, M. S. and Venkataraman, C.: Inventory of aerosol and sulphur dioxide emissions from India. Part II—biomass combustion, Atmos. Env., 36, 699–712, 2002b.

Scarino, A. J., Obland, M. D., Fast, J. D., Burton, S. P., Ferrare, R. A., Hostetler, C. A., Berg, L. K., Lefer, B., Haman, C., Hair, J. W., Rogers, R. R., Butler, C., Cook, A. L. and Harper, D. B.: Comparison of mixed layer heights from airborne high spectral resolution lidar, ground-based measurements, and the WRF-Chem model during CalNex and CARES, Atmos. Chem. Phys. Discuss., 13, 13721-13772, doi:10.5194/acpd-13-13721-2013, 2013.

Seibert, P., Beyrich, F., Gryning, S. E., Joffre, S., Rasmussen, A. and Tercier, Ph.: Review and intercomparison of operational methods for the determination of the mixing height, Atmos , 34, 1001–1027, 2000.

Seidel, D.J., Ao, C.O., Li, K.: Estimating climatological planetary boundary layer heights from radiosonde observations: Comparison of methods and uncertainty analysis. Journal of Geophysical Research 115. https://doi.org/10.1029/2009JD013680, 2010.

Shin, H.H. and Hong, S.-Y.: Intercomparison of planetary boundary-layer parameterizations in the WRF model for a single day from CASES-99. Boundary-Layer Meteorol, 139, 261–281, 2011.

Skamarock, W.C., Klemp, J.B., Dudhia, J., Gill, D.O., Barker, D.M., Wang, W., Powers, J.G.: A description of the advanced research WRF version 2. National Center For Atmospheric Research Boulder Co Mesoscale and Microscale Meteorology Div, 2005.

Sorbjan, Z.: Structure of the Atmospheric Boundary Layer, 317 pp., Prentice Hall, Englewood Cliffs, N.J., 1989.

Sharma S., Vaishnav R., Shukla M.V., Kumar P., Kumar P., Thapliyal P.K., Lal S., Acharya Y.B.: Evaluation of cloud base height measurements from Ceilometer CL31 and MODIS satellite over Ahmedabad, India, Atms, Meas. Tech., 9, 711-719, doi:10.5194/amt-9-711-2016, 2016.

Stull, R. B.: An Introduction to Boundary Layer Meteorology, 666 pp., Dordrecht, Kluwer, 1988.

Summa, D., Di Girolamo, P., Stelitano, D. and Cacciani, M.: Characterization of the planetary boundary layer height and structure by Raman lidar: comparison of different approaches, Atmos. Meas. Tech. Discuss., 6, 5195-5216, doi:10.5194/amtd-6-5195-2013, 2013.

Teixeira, J., Stevens, B. Bretherton, C. S., Cederwall, R. Doyle, J. D., Golaz, J. C ., Holtslag, A. A. M., Klein, S. A ., Lundquist, J. K., Randall, D. A., Siebesma, A. P., Soares, P. M. M.: The parameterization of the atmospheric boundary layer: A view from just above the inversion. Bull. Amer. Meteor. Soc., 89, 453–458, 2008.

Thompson, G., Field, P.R., Rasmussen, R.M., Hall, W.D.: Explicit Forecasts of Winter Precipitation Using an Improved Bulk Microphysics Scheme. Part II: Implementation of a New Snow Parameterization. Monthly Weather Review 136, 5095–5115. https://doi.org/10.1175/2008MWR2387.1, 2008.

Tombrou, M., Dandou, A., Helmis, C., Akylas, E., Aggelopoulos, G., Flocas, H., Assimakopoulos, V.,

Formatted: English (United States)

Formatted: Font color: Auto

Soulakellis N.: 'Model evaluation of the atmospheric boundary layer and Mixed-layer evolution', Boundary-Layer Meteorology, 124, 61-79, 2007

Tsaknakis, G., Papayannis, A., Kokkalis, P., Amiridis, V., Kambezidis, H.D., Mamouri, R.E., Georgoussis, G., Avdikos, G.: Inter-comparison of lidar and ceilometer retrievals for aerosol and Planetary Boundary Layer profiling over Athens, Greece. Atmospheric Measurement Techniques 4, 1261–1273. https://doi.org/10.5194/amt-4-1261-2011, 2011.

Vaughan, M.A., Young, S.A., Winker, D.M., Powell, K.A., Omar, A.H., Liu, Z., Hu, Y., Hostetler, C.A.: Fully automated analysis of space-based lidar data: an overview of the CALIPSO retrieval algorithms and data products, in: Singh, U.N. (Ed.), . p. 16. https://doi.org/10.1117/12.572024, 2004.

Vickers, D., L. Mahrt, L.: The cospectral gap and turbulent flux calculations. J. Atmos. Oceanic Technol., 20, 627–660, 2003.

Vickers D., Mahrt L. 2004. Evaluating formulations of ~~Viterbo, P., Beljaars, A. C.~~ ~~M., Mahouf, J.-F. and Teixeira, J: The representation of soil moisture freezing and its impact on the~~ stable boundary layer height~~, Q.~~ J. Appl~~R.~~ Meteorol. 43: 1736–1749~~Soc., 125, 2401-2426, 1999.~~

Von Engeln A. and Teixeira J.: A Planetary Bpundary Layer Height Climatology Derived from ECMWF Reanalysis Data. J. Climate. 6575-6590, 26, 17, 2013

Voudouri K.A., Giannakaki E., Komppula M., Balis D.: First results of cirrus clouds properties by means of a Polly^{XT} Raman lidar at two measurements sites, EPJ Web of Conferences, 176, 05031, https://doi.org/10.1051/epjconf/201817605031, 2018.

~~Vogelezang, Holtslag: Evaluation and modern impacts of alternative boundary layer height formulations. Bound. Layer Meteor. 81, 245-269, 1996.~~

Wang, K. C., Dickinson, R. E., and Shunlin, L.: Clear sky visibility has decreased over land globally from 1973 to 2007, Science, 323, 1468–1470, doi:10.1126/science.1167549, 2009.

Wang, X.Y., Wang, K.C.: Estimation of atmospheric mixing layer height from radiosonde data. Atmos. Meas. Tech.~~Atmospheric Measurement Techniques~~ 7, 1701–1709. https://doi.org/10.5194/amt-7-1701-2014, 2014.

Wilcoxon, F.: Individual comparison by ranking methods. Biometrics, 1:80-83, 1945.

Wilcoxon, F and Wilcox, R.A.: Some Rapid Approximate Statistical Procedures, Pearl River, New York: Lederle Laboratories, Division of the American Cyanamid Company, 1964.

Wang W., Gong W., Mao F, Pan Z.: An Improved Iterative Fitting Method to Estimate Nocturnal Residual Layer Height. Atmosphere 7(8), 106. https://doi.org/10.3390/atmos7080106, 2016.

Wiegner M., Madonna F., Binietoglou I., Forkel R., Gasteiger J., Geiß A., Pappalardo G., Schäfer K., Thomas W.: What is the benefit of ceilometers for aerosol remote sensing? An answer from EARLINET. Atm. Meas. Tech. 7, 1979-199. doi:10.5194/amt-7-1979-2014, 2014.

Winker, D.H.: CALIOP Algorithm Theoretical Basis. In: CALIOP Instrument, and Algorithms Overview. NASA, 2006.

Zilitinkevich, Sergej, Baklanov, Alexander: Calculation of the Height of Stable Boundary Layers in Operational Models. Danish Meteorological Institute, Copenhagen, 2001.

Formatted: Font color: Auto

Formatted: Font color: Auto

Formatted: Font color: Auto

Formatted: Font color: Auto

Formatted: Font color: Text 1

Formatted: English (United States)

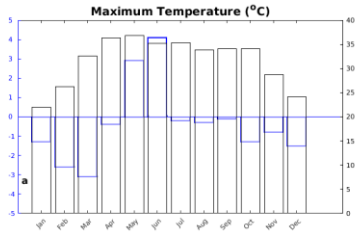

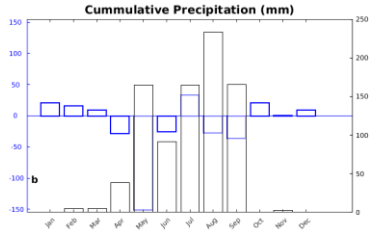

Table 1: The data sources used in this study, spatiotemporal resolution and the corresponding PBL determination method.

Method	Temporal resolution	Vertical resolution	Horizontal resolution	PBL height determination
Raman lidar FMI Polly^{XT}	15min averages of 30sec scans	30m	point measurement	maximum mixing height via aerosol layer top height
CALIOP aboard CALIPSO	16-day repeat cycle	30m	5km	Feature Detection and Layer Properties Algorithm
Radiosondes	12 h	minimum 50 m	point measurement	BRN (Ricr=0.21)
ECMWF	3h	62 pressure levels	1.0° (≈ 100km)	BRN (Ricr=0.25)
WRF	1h	37 Eta levels up to 50hPa	0.02° (≈ 2km)	BRN (Ricr=0.25 over land)

~~**Table 3:** As in Table 2, but for daytime (12:00 UTC).~~

Figure 1: Maximum temperature and cumulative~~total~~ precipitation during the measurement campaign (black) and anomalies (blue)~~anomaly~~ at New Delhi on a monthly basis. Anomalies represent~~The bars indicate the~~ difference between the climatological values and the corresponding values during the measurement campaign. Climatological values were obtained from World Meteorological Organization (http://worldweather.wmo.int/en/city.html?cityId=224) for the site of Safdarjung airport.

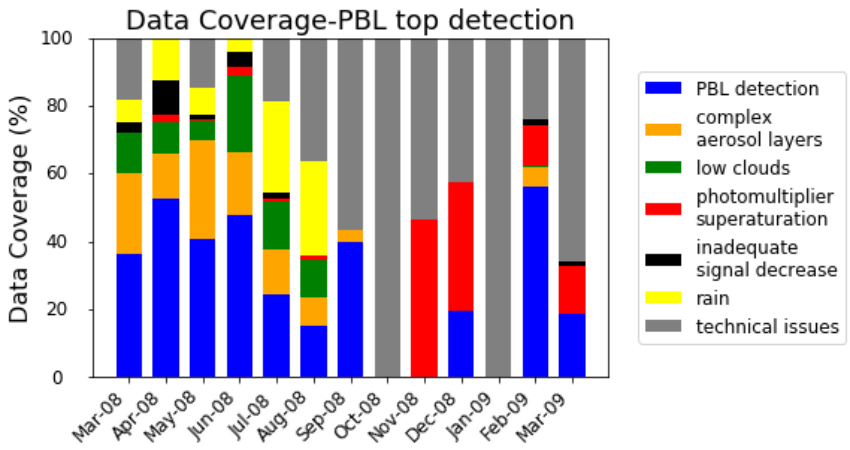

Figure 2: Data coverage of lidar measurements ~~during March 2008-March 2009 classified into seven different categories. Coverage is~~ calculated with respect to total convective hours (from 4 h after sunrise to 1 h before sunset) during the measurement days of the campaign.

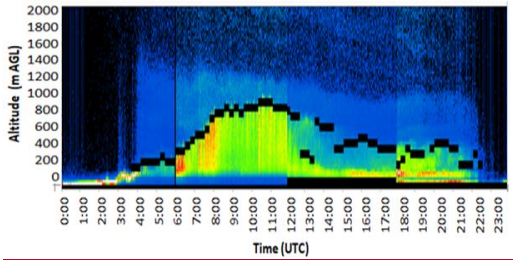

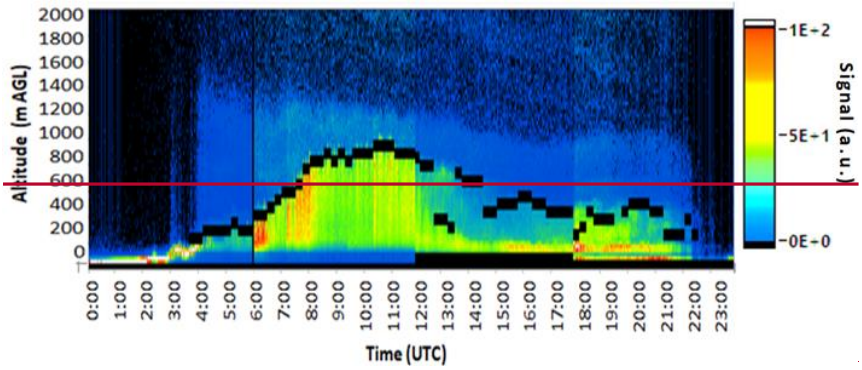

1000

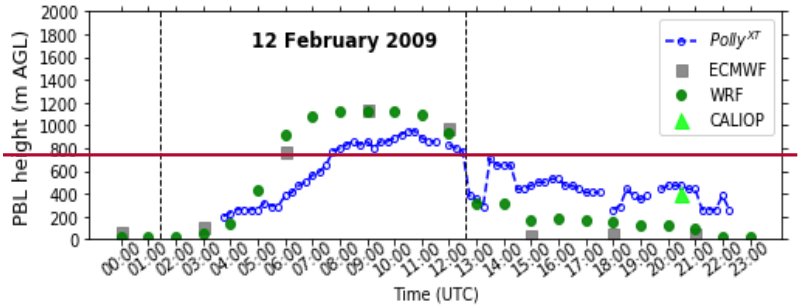

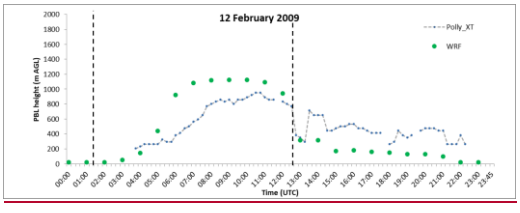

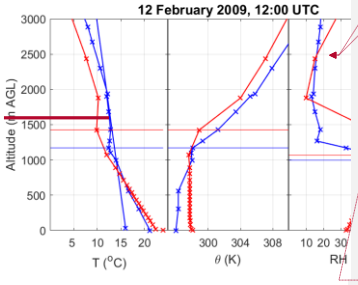

Formatted: Normal

Formatted Table

Formatted: English (United Kingdom)

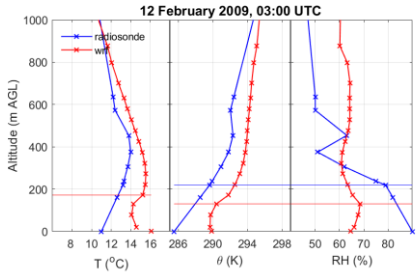

Figure 3: Evolution of PBLH~~PBL height~~ observed on 12 February 2009. Range-corrected signal (top) at 1064 nm as measured with FMI-Polly^{XT}. Black ~~(black~~ lines indicate 15~~-~~-min PBLH, while black zones in the lower part~~values~~ of the figure indicate the extent of the signal cut-off area. The colorscale is normalized on a 6-hour basis, with red and yellow indicating higher aerosol load, while green and blue lower load, respectively. PBLH (bottom) as ~~PBL height). PBL height (middle) as~~ given by the FMI-Polly^{XT}~~, ECMWF, WRF~~ and WRF~~CALIOP~~ (vertical lines indicate sunrise and sunset times). ~~Vertical profiles of T, θ and RH (bottom) as determined by WRF model and radiosonde data (horizontal lines show the PBL height).~~

Formatted: English (United Kingdom)

Formatted: Normal

Formatted: Superscript

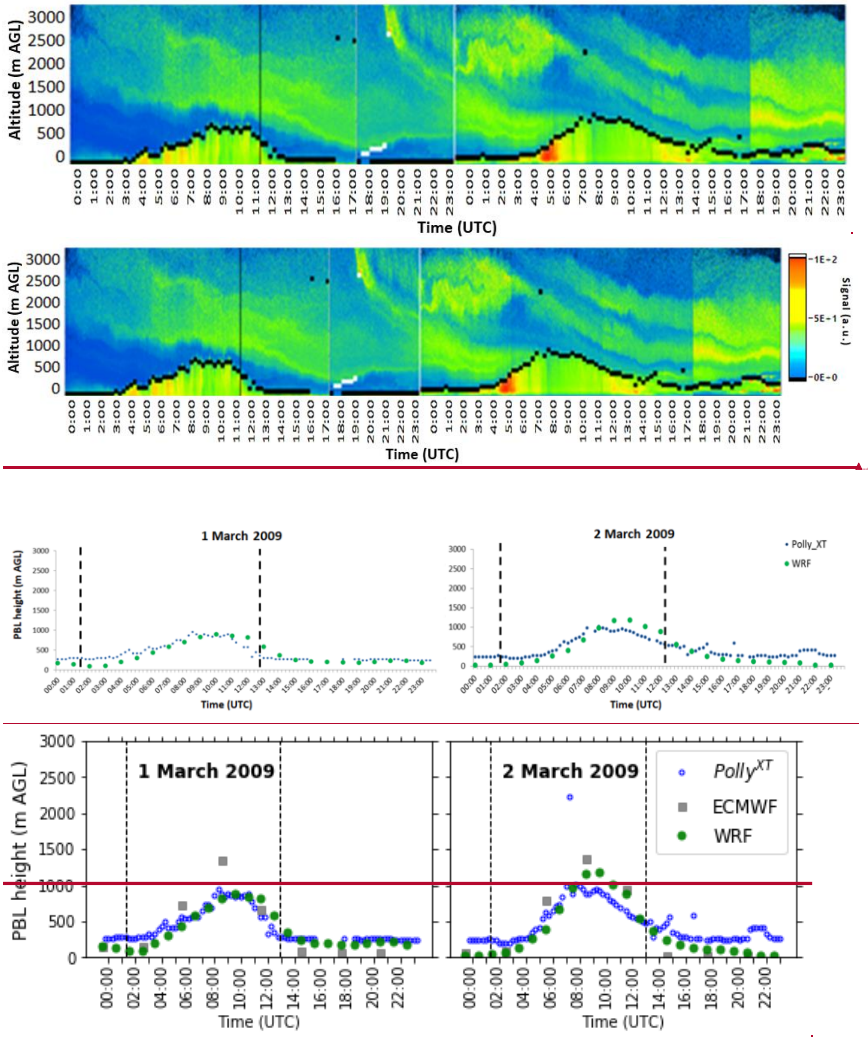

Figure 4: Same as Fig. 3 except for 1-2 March 2009. White horizontal lines (top) indicate 15-min ~~values of~~ cloud base height.

Formatted: German (Germany), Check spelling and

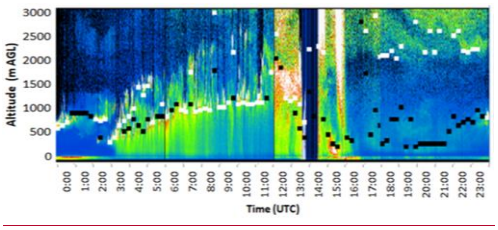

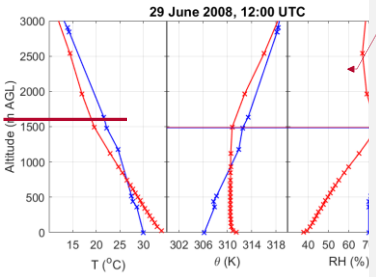

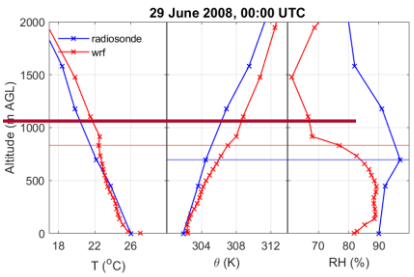

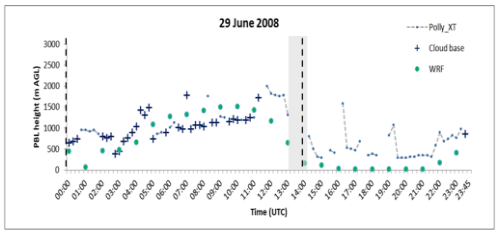

Figure 5: Same as Fig. 3 except for 29 June 2008. ~~White horizontal lines (top) indicate 15-min values of cloud base height.~~ Grey shading (middle) indicates rainfall.

Formatted Table

Formatted: Greek

Formatted: Left

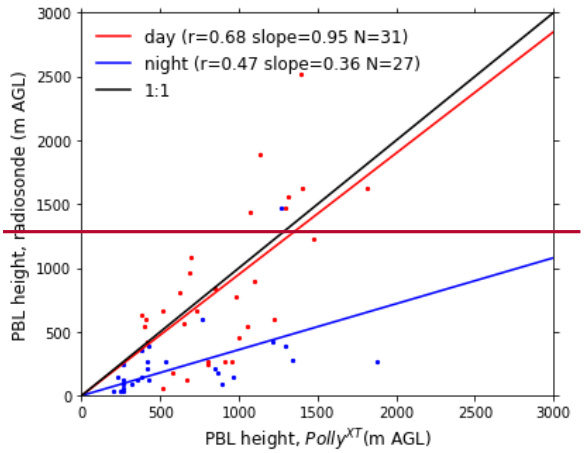

Figure 6: Scatter plots for comparison of FMI-Polly^{XT} to daytime (12:00 UTC) and night-time (00:00 UTC) radiosonde observations throughout the measurement campaign.

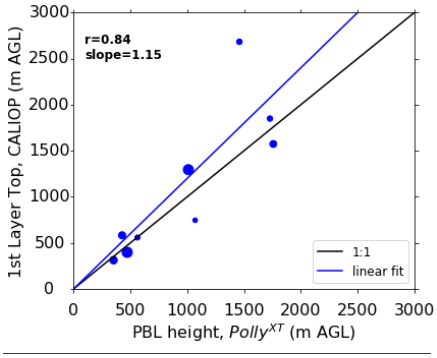

Figure 6: PBLH~~7: PBL top height~~ comparison ~~of 9 common cases~~ for FMI-Polly^{XT} and CALIOP ~~data~~. The heights given by CALIOP have been corrected with elevation. The markersize is proportional to the overpass distance from the ground-based lidar.~~, with a range of 20-101 km.~~

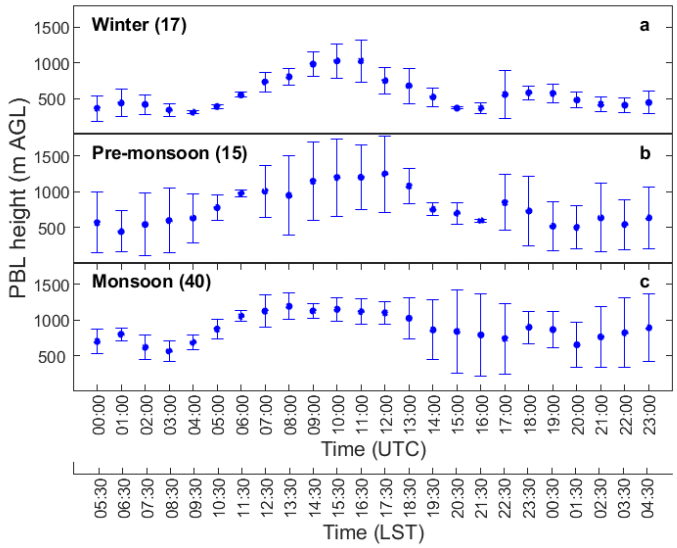
Winter (17)
a
Pre-monsoon (15)
b
Monsoon (40)
c
PBL height (m AGL)
1500
1000
500
00:00
01:00
02:00
03:00
04:00
05:00
06:00
07:00
08:00
09:00
10:00
11:00
12:00
13:00
14:00
15:00
16:00
17:00
18:00
19:00
20:00
21:00
22:00
23:00
Time (UTC)
05:30
06:30
07:30
08:30
09:30
10:30
11:30
12:30
13:30
14:30
15:30
16:30
17:30
18:30
19:30
20:30
21:30
22:30
23:30
00:30
01:30
02:30
03:30
04:30
Time (LST)

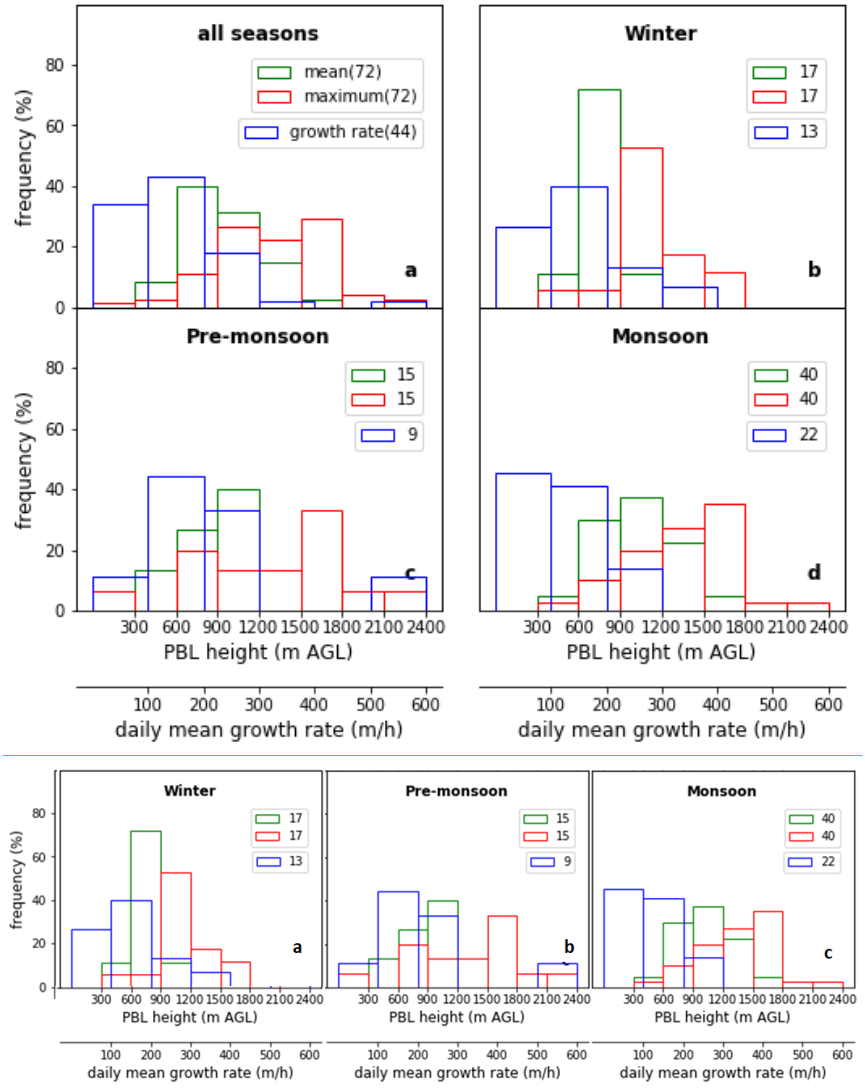

Figure 89: Frequency distribution of daily mean (green) PBLH, daily and maximum PBLH (red) and daily mean growth rate (blue)~~PBL height~~ as calculated during~~throughout~~ the ~~measurement period (a), the~~ winter period (a~~b~~), the pre-monsoon season (b~~e~~) and the monsoon period (c~~d~~). Numbers indicate data availability.

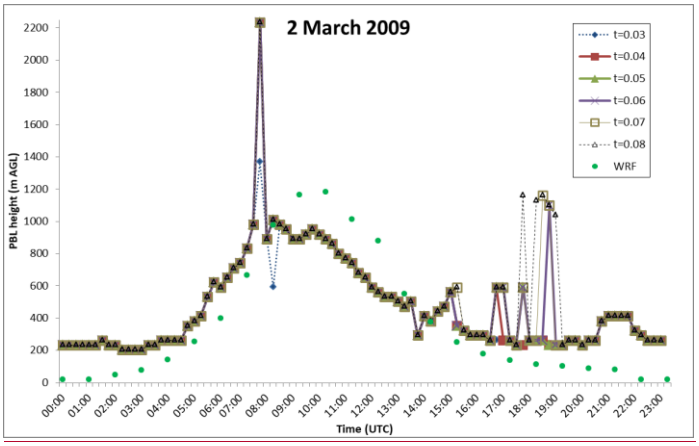

Figure 9: Sensitivity analysis of the WCT method for the case of 2 March 2009. PBLH was estimated by FMI-Polly^{XT}, after modification of the WCT threshold, and by WRF model.